

A mesoscopic ring as a XNOR gate: An exact result

Santanu K. Maiti^{1,2,*}

¹*Theoretical Condensed Matter Physics Division, Saha Institute of Nuclear Physics,
1/AF, Bidhannagar, Kolkata-700 064, India*

²*Department of Physics, Narasinha Dutt College, 129, Belilious Road, Howrah-711 101, India*

Abstract

We describe XNOR gate response in a mesoscopic ring threaded by a magnetic flux ϕ . The ring is attached symmetrically to two semi-infinite one-dimensional metallic electrodes and two gate voltages, viz, V_a and V_b , are applied in one arm of the ring which are treated as the inputs of the XNOR gate. The calculations are based on the tight-binding model and the Green's function method, which numerically compute the conductance-energy and current-voltage characteristics as functions of the ring-to-electrode coupling strength, magnetic flux and gate voltages. Our theoretical study shows that, for a particular value of ϕ ($= \phi_0/2$) ($\phi_0 = ch/e$, the elementary flux-quantum), a high output current (1) (in the logical sense) appears if both the two inputs to the gate are the same, while if one but not both inputs are high (1), a low output current (0) results. It clearly exhibits the XNOR gate behavior and this aspect may be utilized in designing an electronic logic gate.

PACS No.: 73.23.-b; 73.63.Rt.

Keywords: Mesoscopic ring; Conductance; I - V characteristic; XNOR gate

***Corresponding Author:** Santanu K. Maiti
Electronic mail: santanu.maiti@saha.ac.in

1 Introduction

Low-dimensional model quantum confined systems have been the key objects of both theoretical and experimental research, mainly due to the fact that these simple looking systems are prospective candidates for nanodevices in electronic as well as spintronic engineering. The study of electron transport in such systems has become one of the most fascinating branch of nanoscience and technology. The idea of manufacturing nanodevices are based on the concept of quantum interference effect. For much smaller sizes the quantum phase coherence is maintained across the sample, while it generally disappears for larger systems. A mesoscopic metallic ring is one such promising example where electronic motion is confined and the transport becomes predominantly coherent. With the help of a mesoscopic ring, we can make an electronic device that can be operated as a logic gate, which may be used in nanoelectronic circuits. To explore this phenomenon we design a bridge system where the ring is sandwiched between two external electrodes, the so-called electrode-ring-electrode bridge. The ring is then subjected to an Aharonov-Bohm (AB) flux ϕ which is the key controlling factor for the whole logical operation in this particular geometry. Following the pioneering work of Aviram and Ratner,¹ the theoretical description of electron transport in a bridge system has got much progress. Later, many excellent experiments²⁻⁴ have been done in several bridge systems to understand the basic mechanisms underlying the electron transport. Though extensive studies on electron transport have already been done both theoretically⁵⁻¹² as well as experimentally,²⁻⁴ yet lot of controversies are still present between the theory and experiment, and the complete knowledge of the conduction mechanism in this scale is not very well established even today. For illustrative purposes, here we mention some of these issues as follow. The electronic transport in the ring changes drastically depending on the interface geometry between the ring and the electrodes. By changing the geometry, one can tune the transmission probability of an electron across the ring which is solely due to the effect of quantum interference among the electronic waves passing through different arms of the ring. Not only that, the electron transport in the ring can be modulated in other way by tuning the magnetic flux, that threads the ring. The AB flux threading the ring may change the phases of the wave functions propagating along the differ-

ent arms of the ring leading to constructive or destructive interferences, and therefore, the transmission amplitude changes.¹³⁻¹⁷ Beside these factors, ring-to-electrode coupling is another important issue that controls the electron transport in a meaningful way.¹⁷ All these are the key factors which regulate the electron transmission in the electrode-ring-electrode bridge system and they have to be taken into account properly to reveal the transport mechanisms.

Our main aim of the present work is to explore the XNOR gate behavior in a mesoscopic ring threaded by a magnetic flux ϕ . The ring is sandwiched symmetrically between two electrodes, and two gate voltages V_a and V_b are applied in one arm of the ring (see Fig. 1) those are treated as the two inputs of the XNOR gate. A simple tight-binding model is used to describe the system and all the calculations are done numerically. Here we address the XNOR gate behavior by studying the conductance-energy and current-voltage characteristics as functions of the ring-to-electrode coupling strength, magnetic flux and gate voltages. Our exact numerical study reveals that for a particular value of the magnetic flux, $\phi = \phi_0/2$, a high output current (1) (in the logical sense) is available if both the two inputs to the gate are the same (either low or high), while if one but not both inputs are high (1), a low output current (0) appears. This phenomenon clearly shows the XNOR gate behavior. To the best of our knowledge the XNOR gate response in such a simple system has yet not been addressed in the literature.

We arrange the paper as follow. Following the introduction (Section 1), in Section 2, we described the model and the theoretical formulations for the calculation. Section 3 explores the results, and finally, we conclude our study in Section 4.

2 Model and the theoretical background

Let us start with the model presented in Fig. 1. A mesoscopic ring, subjected to an AB flux ϕ , is attached symmetrically (upper and lower arms have equal number of lattice points) to two semi-infinite one-dimensional (1D) metallic electrodes. Two gate voltages V_a and V_b , taken as the two inputs of the XNOR gate, are applied to the atomic sites a and b , respectively, in the upper arm of the ring. While, an additional gate voltage V_α is applied to the site α in the lower arm of the ring. These three voltages

are variable.

At much low temperatures and bias voltage, the conductance g of the ring can be expressed from the Landauer conductance formula,^{18,19}

$$g = \frac{2e^2}{h} T \quad (1)$$

where T gives the transmission probability of an electron across the ring. This (T) can be represented in terms of the Green's function of the ring and its coupling to the two electrodes by the relation,^{18,19}

$$T = Tr [\Gamma_S G_R^r \Gamma_D G_R^a] \quad (2)$$

where G_R^r and G_R^a are respectively the retarded and advanced Green's functions of the ring including the effects of the electrodes. Here Γ_S and Γ_D describe

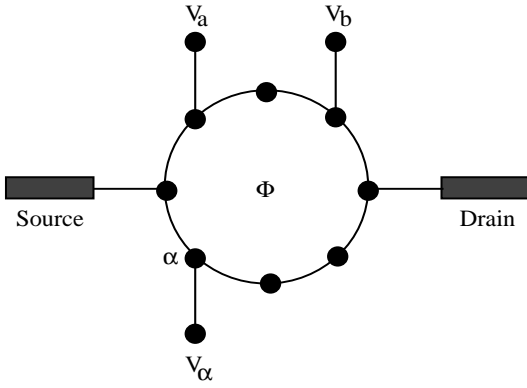


Figure 1: Schematic view for the operation of a XNOR gate. The atomic sites a , b and α are subjected to the voltages V_a , V_b and V_α , respectively, those are variable.

the coupling of the ring to the source and drain, respectively. For the complete system i.e., the ring, source and drain, the Green's function is defined as,

$$G = (E - H)^{-1} \quad (3)$$

where E is the injecting energy of the source electron. To Evaluate this Green's function, the inversion of an infinite matrix is needed since the complete system consists of the finite ring and the two semi-infinite electrodes. However, the entire system can be partitioned into sub-matrices corresponding to the individual sub-systems and the Green's function for the ring can be effectively written as,

$$G_R = (E - H_R - \Sigma_S - \Sigma_D)^{-1} \quad (4)$$

where H_R is the Hamiltonian of the ring. Within the non-interacting picture the Hamiltonian can be expressed in the form,

$$H_R = \sum_i (\epsilon_{i0} + V_a \delta_{ia} + V_b \delta_{ib} + V_\alpha \delta_{i\alpha}) c_i^\dagger c_i + \sum_{\langle ij \rangle} t (c_i^\dagger c_j e^{i\theta} + c_j^\dagger c_i e^{-i\theta}) \quad (5)$$

where ϵ_{i0} 's are the site energies for all the sites i except the sites $i = a, b$ and α where the gate voltages V_a , V_b and V_α are applied, those are variable. These gate voltages can be incorporated through the site energies as expressed in the above Hamiltonian. c_i^\dagger (c_i) is the creation (annihilation) operator of an electron at the site i and t is the nearest-neighbor hopping integral. The phase factor $\theta = 2\pi\phi/N\phi_0$ comes due to the flux ϕ threaded by the ring, where N corresponds to the total number of atomic sites in the ring. A similar kind of tight-binding Hamiltonian is also used, except the phase factor θ , to describe the 1D perfect electrodes where the Hamiltonian is parametrized by constant on-site potential ϵ_0 and nearest-neighbor hopping integral t_0 . The hopping integral between the source and the ring is τ_S , while it is τ_D between the ring and the drain. In Eq. 4, $\Sigma_S = h_{SR}^\dagger g_S h_{SR}$ and $\Sigma_D = h_{DR}^\dagger g_D h_{DR}$ are the self-energy operators due to the two electrodes, where g_S and g_D correspond to the Green's functions of the source and drain, respectively. h_{SR} and h_{DR} are the coupling matrices and they will be non-zero only for the adjacent points of the ring, and the electrodes, respectively. The matrices Γ_S and Γ_D can be calculated through the expression,

$$\Gamma_{S(D)} = i [\Sigma_{S(D)}^r - \Sigma_{S(D)}^a] \quad (6)$$

where $\Sigma_{S(D)}^r$ and $\Sigma_{S(D)}^a$ are the retarded and advanced self-energies, respectively, and they are conjugate with each other. Datta *et al.*²⁰ have shown that the self-energies can be expressed like as,

$$\Sigma_{S(D)}^r = \Lambda_{S(D)} - i\Delta_{S(D)} \quad (7)$$

where $\Lambda_{S(D)}$ are the real parts of the self-energies which correspond to the shift of the energy eigenvalues of the ring and the imaginary parts $\Delta_{S(D)}$ of the self-energies represent the broadening of these energy levels. All the information about the ring-to-electrode coupling are included into these two self-energies.

The current passing through the ring is depicted as a single-electron scattering process between the two reservoirs of charge carriers. The current I can

be computed as a function of the applied bias voltage V by the expression,¹⁸

$$I(V) = \frac{e}{\pi\hbar} \int_{-\infty}^{\infty} (f_S - f_D) T(E) dE \quad (8)$$

where $f_{S(D)} = f(E - \mu_{S(D)})$ gives the Fermi distribution function with the electrochemical potentials $\mu_{S(D)} = E_F \pm eV/2$. Here we assume that the entire voltage is dropped across the ring-electrode interfaces, and it is examined that under such an assumption the I - V characteristics do not change their qualitative features.²⁰

All the results in this communication are done at absolute zero temperature, but they should valid even for finite temperatures (~ 300 K), since the broadening of the energy levels of the ring due to its coupling to the electrodes becomes much larger than that of the thermal broadening.¹⁸ On the other hand, at high temperature limit, all these phenomena completely disappear. This is due to the fact that the phase coherence length decreases significantly with the rise of temperature where the contribution comes mainly from the scattering on phonons, and accordingly, the quantum interference effect vanishes. For simplicity, we take the unit $c = e = \hbar = 1$ in our present calculation.

3 Results and discussion

To illustrate the results, let us first mention the values of the different parameters those are used for the numerical calculation. The on-site energy ϵ_{i0} of the ring is taken as 0 for all the sites i , except the sites $i = a, b$ and α where the site energies are taken as V_a, V_b and V_α , respectively, and the nearest-neighbor hopping strength t is set to 3. On the other hand, for the side attached electrodes the on-site energy (ϵ_0) and the nearest-neighbor hopping strength (t_0) are fixed to 0 and 4, respectively. The voltage V_α is set to 2, and the Fermi energy E_F is fixed at 0 for the whole computation. Throughout the study, we focus our results for the two limiting cases depending on the strength of the coupling of the ring to the side attached electrodes. In one case we use the condition $\tau_{S(D)} \ll t$, which is the so-called weak-coupling limit. For this regime we choose $\tau_S = \tau_D = 0.5$. In the other case the condition $\tau_{S(D)} \sim t$ is used, which is named as the strong-coupling limit. In this particular regime, the values of the parameters are set as $\tau_S = \tau_D = 2.5$. The significant parameter for all these calculations

is the AB flux ϕ which is set to $\phi_0/2$ i.e., 0.5 in our chosen unit.

As illustrative examples, in Fig. 2 we describe the conductance-energy (g - E) characteristics for a mesoscopic ring with $N = 8$ and $V_\alpha = 2$ in the limit of weak-coupling, where (a), (b), (c) and (d) correspond to the results for the different cases of the input voltages, V_a and V_b . For the particular cases where anyone of the two inputs is high and other is low i.e., both the two inputs are not same, the conductance g becomes exactly zero (Figs. 2(b) and (c)) for the whole energy range. This predicts

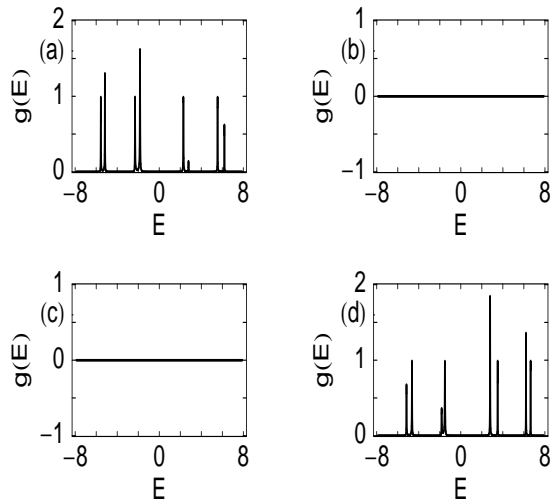


Figure 2: g - E curves in the weak-coupling limit for a mesoscopic ring with $N = 8$, $V_\alpha = 2$ and $\phi = 0.5$. (a) $V_a = V_b = 0$, (b) $V_a = 2$ and $V_b = 0$, (c) $V_a = 0$ and $V_b = 2$ and (d) $V_a = V_b = 2$.

that for these two cases, electron cannot conduct through the ring. The situation becomes completely different for the cases when both the inputs to the gate are the same, either low ($V_a = V_b = 0$) or high ($V_a = V_b = 2$). In these two cases, the conductance shows fine resonant peaks for some particular energies (Figs. 2(a) and (d)), which reveal the electron conduction across the ring. At the resonant energies, g does not get the value 2, and therefore, the transmission probability T becomes less than unity, since the expression $g = 2T$ is satisfied from the Landauer conductance formula (see Eq. 1 with $e = \hbar = 1$). This reduction of the transmission amplitude is due to the effect of quantum interference which we will describe below. All these resonant peaks are associated with the energy eigenvalues of the ring, and thus, it can be predicted that the conductance spectrum manifests itself the elec-

tronic structure of the ring. Hence, more resonant peaks are expected for the larger rings, associated with their energy spectra. Now we discuss the effects of the gate voltages on the electron transport for these four different cases of the input voltages. The transmission probability of getting an electron across the ring depends on the quantum interference of the electronic waves passing through the two arms (upper and lower) of the ring. For the symmetrically connected ring i.e., when the two arms of the ring are identical with each other, the probability amplitude becomes exactly zero ($T = 0$) for the

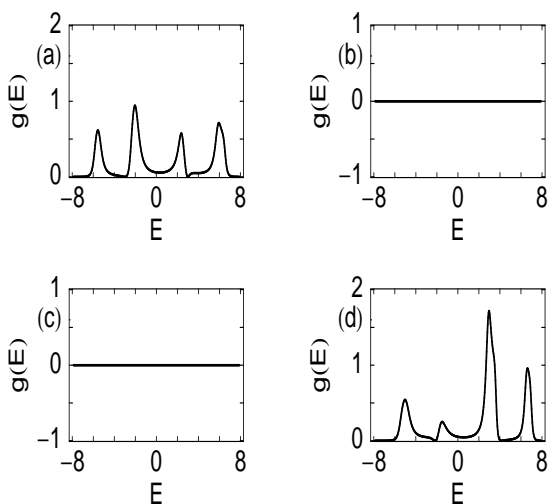


Figure 3: g - E curves in the strong-coupling limit for a mesoscopic ring with $N = 8$, $V_\alpha = 2$ and $\phi = 0.5$. (a) $V_a = V_b = 0$, (b) $V_a = 2$ and $V_b = 0$, (c) $V_a = 0$ and $V_b = 2$ and (d) $V_a = V_b = 2$.

typical flux, $\phi = \phi_0/2$. This is due to the result of the quantum interference among the two waves in the two arms of the ring, which can be established through few simple mathematical steps. Thus, for the cases when anyone of the two inputs to the gate is identical to 2 and other one is 0, the upper and lower arms of the ring become exactly similar. This is because the potential V_α is also set to 2. Accordingly, the transmission probability T drops to zero. If the high value (2) of anyone of the two gates is different from the potential applied in the atomic site α , then the two arms are not identical with each other and the transmission probability will not vanish. Thus, to get the zero transmission probability when V_a is high and V_b is low and vice versa, we should tune V_α properly, observing the input potential. On the other hand, due to the breaking of the symmetry of the two arms, the non-zero value of

the transmission probability is achieved in the particular cases when both the two inputs to the gate are the same, which reveals the electron conduction across the ring. From these results we can emphasize that the electron conduction through the ring takes place if both the two inputs to the gate are the same (low or high), while if one but not both inputs are high, the conduction is no longer possible. This aspect clearly describes the XNOR gate behavior. In addition to these properties here we also mention the effect of the ring-to-electrode coupling. As illustrative examples, in Fig. 3 we plot the g - E characteristics for the strong-coupling limit, where (a), (b), (c) and (d) are drawn respectively for the same input voltages as in Fig. 2. In the strong-coupling limit, all the resonant peaks get substantial widths

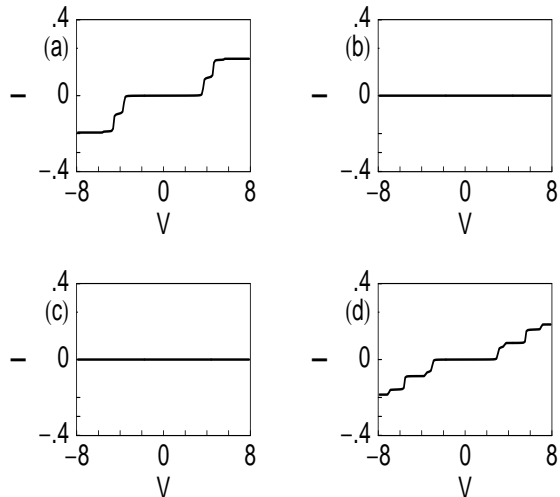


Figure 4: Current I as a function of the bias voltage V for a mesoscopic ring with $N = 8$, $V_\alpha = 2$ and $\phi = 0.5$ in the limit of weak-coupling. (a) $V_a = V_b = 0$, (b) $V_a = 2$ and $V_b = 0$, (c) $V_a = 0$ and $V_b = 2$ and (d) $V_a = V_b = 2$.

compared to the weak-coupling limit. This is due to the broadening of the energy levels of the ring in the limit of strong-coupling, where the contribution comes from the imaginary parts of the self-energies Σ_S and Σ_D , respectively.¹⁸ Therefore, by tuning the coupling strength, we can get the electron transmission across the ring for the wider range of energies and it provides an important behavior in the study of current-voltage (I - V) characteristics. The effects of the gate voltages, V_a and V_b , on the electron transport in the strong-coupling limit remain exactly similar as in the case of weak-coupling limit.

All these features of electron transport become

much more clearly illustrated from our presented current-voltage (I - V) characteristics. The current passing through the ring is determined by integrating the transmission function T as prescribed in Eq. 8. The transmission function varies exactly similar to that of the conductance spectrum, differ only in magnitude by the factor 2 since the relation $g = 2T$ holds from the Landauer conductance formula, Eq. 1. As representative examples, in Fig. 4 we plot the I - V characteristics for a mesoscopic ring with $N = 8$ and $V_\alpha = 2$, in the limit of weak-coupling, where (a), (b), (c) and (d) represent the results for the four different cases of the two input voltages. From these characteristics it is clearly observed that for the cases when one input is high and other is low, the current I becomes exactly zero (see Figs. 4(b) and (c)) for the entire bias voltage V . This phenomenon can be understood from the conductance spectra, Figs. 2(b) and (c),

Table 1: XNOR gate behavior in the limit of weak-coupling. The current I is computed at the bias voltage 6.02.

Input-I (V_a)	Input-II (V_b)	Current (I)
0	0	0.194
2	0	0
0	2	0
2	2	0.157

since the current is computed from the integration method of the transmission function T . The non-zero value of the current appears only when both the two inputs are identical to zero (Fig. 4(a)) or high (Fig. 4(d)). The current exhibits staircase-like structure with fine steps as a function of the applied bias voltage. This is due to the existence of the sharp resonant peaks in the conductance spectrum in the weak-coupling limit, since the current is computed by the integration method of the transmission function T . With the increase of the bias voltage V , the electrochemical potentials on the electrodes are shifted gradually, and finally cross one of the quantized energy levels of the ring. Accordingly, a current channel is opened up which provides a jump in the I - V characteristic curve. Here, it is also important to note that the non-zero value of the current appears beyond a finite value of the bias voltage V , the so-called threshold voltage (V_{th}). This V_{th} can be changed by controlling the size (N) of the ring. From these current-voltage spectra, the XNOR gate

behavior of the ring can be observed very nicely. To make it much more clearer, in Table 1, we show a quantitative estimate of the typical current amplitude determined at the bias voltage $V = 6.02$. It shows that, when both the two inputs to the gate are zero, the current gets the value 0.194. While, it (I) achieves 0.157 for the case when the two inputs are identical to 2. On the other hand, for the other two cases, the current becomes exactly zero. In the same fashion, as above, here we also describe the

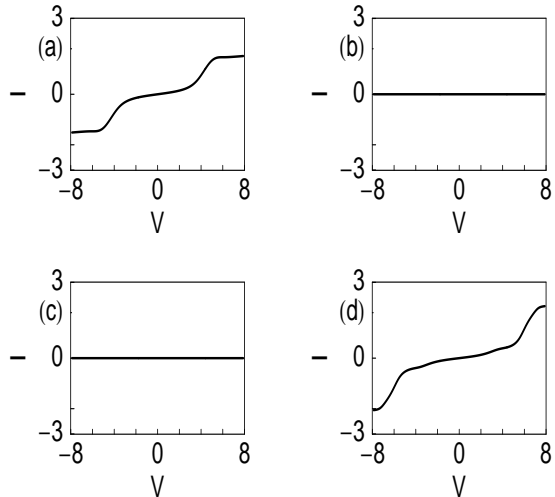


Figure 5: Current I as a function of the bias voltage V for a mesoscopic ring with $N = 8$, $V_\alpha = 2$ and $\phi = 0.5$ in the limit of strong-coupling. (a) $V_a = V_b = 0$, (b) $V_a = 2$ and $V_b = 0$, (c) $V_a = 0$ and $V_b = 2$ and (d) $V_a = V_b = 2$.

I - V characteristics for the limit of strong-coupling. In this limit, the current varies almost continuously with the applied bias voltage and gets much larger amplitude than the weak-coupling case (Fig. 4), as presented in Fig. 5. The fact is that, in the limit of strong-coupling all the resonant peaks get broadened which provide larger current in the integration procedure of the transmission function T . Thus by tuning the strength of the ring-to-electrode coupling, we can achieve very large current amplitude from the very low one for the same bias voltage V . All the other properties i.e., the dependences of the gate voltages on the I - V characteristics are exactly similar to those as given in Fig. 4. In this strong-coupling limit we also make a quantitative study for the typical current amplitude, given in Table 2, where the current amplitude is determined at the same bias voltage ($V = 6.02$) as earlier. The response of the output current is exactly similar to

that as given in Table 1. Here the current gets the value 1.466 for the case when $V_a = V_b = 0$, and, it goes to 1.174 when $V_a = V_b = 2$. While, the current exactly vanishes for the other two cases. The non-zero values of the current in this strong-coupling

Table 2: XNOR gate behavior in the limit of strong-coupling. The current I is computed at the bias voltage 6.02.

Input-I (V_a)	Input-II (V_b)	Current (I)
0	0	1.466
2	0	0
0	2	0
2	2	1.174

limit are much larger than the weak-coupling case, as expected. From these results we can clearly manifest that a mesoscopic ring exhibits the XNOR gate response.

4 Concluding remarks

In this presentation, we have discussed the XNOR gate behavior of a mesoscopic metallic ring threaded by a magnetic flux ϕ in the Green's function formalism. The ring is attached symmetrically to the electrodes and two gate voltages V_a and V_b are applied in one arm of the ring which are taken as the inputs of the XNOR gate. A simple tight-binding model is used to describe the system and all the calculations are done numerically. We have computed the conductance-energy and current-voltage characteristics as functions of the gate voltages, ring-to-electrode coupling strength and magnetic flux. Very interestingly we have observed that, for the half flux-quantum value of ϕ ($\phi = \phi_0/2$), a high output current (1) (in the logical sense) appears if both the two inputs to the gate are the same, either low (0) or high (1). While, if anyone of the two inputs is high (1) and other is low (0), a low output current (0) results. It clearly manifests the XNOR gate behavior and this aspect may be utilized in designing a tailor made electronic logic gate.

Throughout our study, we have addressed the conductance-energy and current-voltage characteristics for some fixed parameter values considering a ring with total number of atomic sites $N = 8$. Though the results presented here change numerically for the other parameter values and ring size

(N), but all the basic features remain exactly invariant.

In the present work we have done all the calculations by ignoring the effects of the temperature, electron-electron correlation, disorder, etc. Due to these factors, any scattering process that appears in the arms of the rings would have influence on electronic phases, and, in consequences can disturb the quantum interference effects. Here we have assumed that in our sample all these effects are too small, and accordingly, we have neglected all these factors in this particular study. Beside these factors, in the present study we have also ignored the effect of Al'tshuler, Aronov and Spivak (AAS) oscillation. The AAS oscillation will appear when either a large amount of fluctuations is introduced in the site energies of the ring or the electronic mean free path becomes much smaller than the ring size. But, in our model, since there is no such fluctuations and also the electronic mean free path is comparable to the system size, the effect of AAS oscillation will no longer be observed.

The importance of this presentation is mainly concerned with (i) the simplicity of the geometry and (ii) the smallness of the size. To the best of our knowledge the XNOR gate response in such a simple low-dimensional system that can be operated even at finite temperatures (~ 300 K) has not been addressed earlier in the literature.

Acknowledgment

I am grateful to the Physical Society of Japan for financial support in publication.

References

- [1] A. Aviram and M. Ratner: Chem. Phys. Lett. **29** (1974) 277.
- [2] J. Chen, M. A. Reed, A. M. Rawlett, and J. M. Tour: Science **286** (1999) 1550.
- [3] M. A. Reed, C. Zhou, C. J. Muller, T. P. Burgin, and J. M. Tour: Science **278** (1997) 252.
- [4] T. Dadoosh, Y. Gordin, R. Krahne, I. Khivrich, D. Mahalu, V. Frydman, J. Sperling, A. Yacoby, and I. Bar-Joseph: Nature **436** (2005) 677.

- [5] P. A. Orellana, M. L. Ladron de Guevara, M. Pacheco, and A. Latge: Phys. Rev. B **68** (2003) 195321.
- [6] P. A. Orellana, F. Dominguez-Adame, I. Gomez, and M. L. Ladron de Guevara: Phys. Rev. B **67** (2003) 085321.
- [7] A. Nitzan: Annu. Rev. Phys. Chem. **52** (2001) 681.
- [8] A. Nitzan and M. A. Ratner: Science **300** (2003) 1384.
- [9] V. Mujica, M. Kemp, and M. A. Ratner: J. Chem. Phys. **101** (1994) 6849.
- [10] V. Mujica, M. Kemp, A. E. Roitberg, and M. A. Ratner: J. Chem. Phys. **104** (1996) 7296.
- [11] K. Walczak: Phys. Stat. Sol. (b) **241** (2004) 2555.
- [12] K. Walczak: arXiv:0309666.
- [13] R. Baer and D. Neuhauser: J. Am. Chem. Soc. **124** (2002) 4200.
- [14] D. Walter, D. Neuhauser, and R. Baer: Chem. Phys. **299** (2004) 139.
- [15] K. Tagami, L. Wang, and M. Tsukada: Nano Lett. **4** (2004) 209.
- [16] K. Walczak: Cent. Eur. J. Chem. **2** (2004) 524.
- [17] R. Baer and D. Neuhauser: Chem. Phys. **281** (2002) 353.
- [18] S. Datta: *Electronic transport in mesoscopic systems*, Cambridge University Press, Cambridge (1997).
- [19] M. B. Nardelli: Phys. Rev. B **60** (1999) 7828.
- [20] W. Tian, S. Datta, S. Hong, R. Reifenberger, J. I. Henderson, and C. I. Kubiak: J. Chem. Phys. **109** (1998) 2874.